ARTICLES
https://doi.org/10.1038/s41557-019-0290-1
nature chemistry

Kinetic modulation of graphene growth by fluorine through spatially confined decomposition of metal fluorides

Can Liu[1,2,13], Xiaozhi Xu[1,3,13], Lu Qiu[4,5,13], Muhong Wu[1,6,13], Ruixi Qiao[1], Li Wang[1,7], Jinhuan Wang[1], Jingjing Niu[1], Jing Liang[1], Xu Zhou[1,2], Zhihong Zhang[1], Mi Peng[8], Peng Gao[9,10], Wenlong Wang[7], Xuedong Bai[7], Ding Ma[8], Ying Jiang[9], Xiaosong Wu[1], Dapeng Yu[11,12], Enge Wang[6,9], Jie Xiong[2*], Feng Ding[4,5*] and Kaihui Liu[1,10*]

Two-dimensional materials show a variety of promising properties, and controlling their growth is an important aspect for practical applications. To this end, active species such as hydrogen and oxygen are commonly introduced into reactors to promote the synthesis of two-dimensional materials with specific characteristics. Here, we demonstrate that fluorine can play a crucial role in tuning the growth kinetics of three representative two-dimensional materials (graphene, hexagonal boron nitride and WS_2). When growing graphene by chemical vapour deposition on a copper foil, fluorine released from the decomposition of a metal fluoride placed near the copper foil greatly accelerates the growth of the graphene (up to a rate of ~200 μm s^{-1}). Theoretical calculations show that it does so by promoting decomposition of the methane feedstock, which converts the endothermic growth process to an exothermic one. We further show that the presence of fluorine also accelerates the growth of two-dimensional hexagonal boron nitride and WS_2.

During the growth of graphene and other two-dimensional (2D) materials, the presence of hydrogen and oxygen is known to be critical for processes such as ultrafast growth[1], nucleation suppression[2] and layer number control[3]. Owing to its high electronegativity, fluorine—known to greatly affect a variety of reactions[4–9], especially in organic chemistry—is also expected to enable tuning of the growth of 2D materials. Although it has previously been involved in post-growth treatments[10–12], fluorine has not yet been directly involved in growth processes due to the following difficulties: (1) its high reactivity with reactors, which are typically composed of glass and rubber (even a small amount of fluorine can cause damage) and (2) the high toxicity of the by-products potentially generated, such as hydrogen fluoride.

In contrast to traditional bulk material growth, most key reactions in the bottom-up synthesis of 2D materials, such as in chemical vapour deposition (CVD), occur near the surface of the substrate. Only a limited amount of reactants are therefore required to feed the growth of a 2D material, which is normally one atom or a few atoms thick. Based on this unique aspect, we propose to use spatially confined decomposition of metal fluoride as the local fluorine source to modulate the reaction of 2D material growth. As 2D material growth is essentially a surface-reaction process, the amount of fluorine released from the metal fluoride in the confined space is sufficient to modulate the reactions without any observable damage to the reactor.

In this article, we investigate fluorine-modulated 2D material growth using graphene, hexagonal boron nitride (h-BN) and WS_2 (a conductor, an insulator and a semiconductor, respectively) as three representative examples. All three materials have attractive properties[13–15] and broad applications[16–23], and their syntheses have been extensively investigated[24–48]. With a carefully designed local fluorine feeding system based on the spatially confined decomposition of metal fluoride, the growth kinetics of graphene were observed to change dramatically: the barrier of methane (CH_4) decomposition was greatly reduced through fluorine substitution, and the reaction was switched from endothermic to exothermic. As a consequence, sufficient carbon precursor feeding led to a high growth rate of ~200 μm s^{-1}. During the synthesis of h-BN and WS_2 through CVD processes, the presence of local fluorine was also found to significantly increase the growth rate. Our work therefore demonstrates that fluorine can serve to modulate the growth kinetics, and accelerates the growth of graphene and other 2D materials.

Results

Local fluorine-modulated graphene growth. Oxygen can be released from the oxide surface at high temperature becuase of the

[1]State Key Laboratory for Mesoscopic Physics, Academy for Advanced Interdisciplinary Studies, School of Physics, Peking University, Beijing, China. [2]State Key Laboratory of Electronic Thin Films and Integrated Devices, University of Electronic Science and Technology of China, Chengdu, China. [3]School of Physics and Telecommunication Engineering, South China Normal University, Guangzhou, China. [4]Centre for Multidimensional Carbon Materials, Institute for Basic Science, Ulsan, Republic of Korea. [5]School of Materials Science and Engineering, Ulsan National Institute of Science and Technology, Ulsan, Republic of Korea. [6]Songshan Lake Materials Laboratory, Dongguan, Guangdong, China. [7]Beijing National Laboratory for Condensed Matter Physics, Institute of Physics, Chinese Academy of Sciences, Beijing, China. [8]Beijing National Laboratory for Molecular Sciences, College of Chemistry and Molecular Engineering and College of Engineering, and BIC-ESAT, Peking University, Beijing, China. [9]International Centre for Quantum Materials, Peking University, Beijing, China. [10]Collaborative Innovation Centre of Quantum Matter, Beijing, China. [11]Institute for Quantum Science and Engineering and Department of Physics, South University of Science and Technology of China, Shenzhen, China. [12]Shenzhen Key Laboratory of Quantum Science and Engineering, Shenzhen, China. [13]These authors contributed equally: Can Liu, Xiaozhi Xu, Lu Qiu, Muhong Wu. *e-mail: jiexiong@uestc.edu.cn; f.ding@unist.ac.kr; khliu@pku.edu.cn

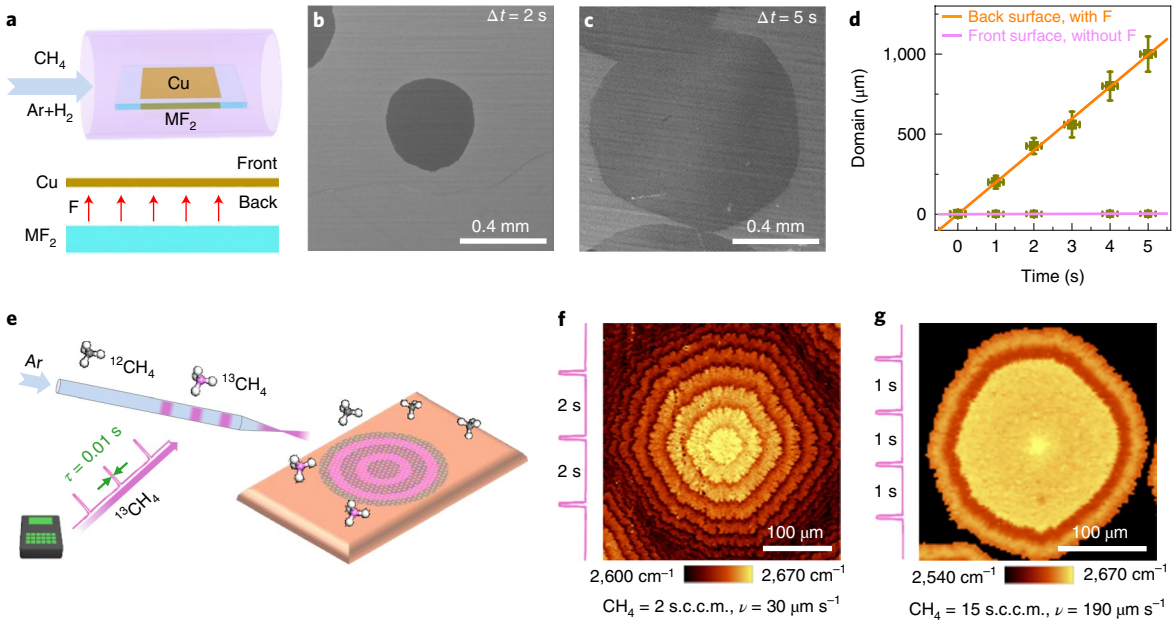

Fig. 1 | Graphene growth modulated by local fluorine. a, Schematics of the experimental design. The copper foil is placed directly above a metal fluoride substrate (MF_2; M = Ba, Ca or Mg) with a small gap of 10–20 μm. At high temperatures, some fluorine radicals are released from the metal fluoride surface to the gap between the copper foil and metal fluoride. **b**,**c**, SEM images of graphene domains growing at $\Delta t = 2$ s (**b**) and $\Delta t = 5$ s (**c**). **d**, Time evolution of the graphene domain diameter. The slope shows a very fast growth rate of ~200 μm s^{-1} with fluorine supply. Error bars represent standard deviations from measurements of 20 samples. **e**, Illustration of our experimental design for programmable transient $^{13}CH_4$ feeding. The Cu foil is exposed to a continuous $^{12}CH_4$ atmosphere, while $^{13}CH_4$ is pulsed (10 ms pulse width) onto the Cu foil through a small nozzle. Ar serves as the carrier gas to better separate the $^{13}CH_4$ sequences. **f**,**g**, Isotope-labelled Raman mappings of the 2D band for graphene domains transferred onto SiO_2/Si substrates growing at different CH_4 fluxes of 2 s.c.c.m. (**f**) and 15 s.c.c.m. (**g**). Dark rings correspond to regions of graphene formed by ^{13}C.

ubiquitous unstable dangling bonds on the material surface. To show that fluorine can also be released at fluoride surfaces under temperatures at which 2D materials are typically grown, the element composition of a thin BaF_2 film (10 nm thick) on a Si substrate was determined before and after annealing at ~1,000 °C, using X-ray photoelectron spectroscopy (XPS). The absence of a fluorine peak after annealing unambiguously demonstrated the release of fluorine from the BaF_2 film (Supplementary Fig. 1).

In our experiment for graphene growth, a copper foil to be used as a substrate for the growth of graphene was directly placed above a BaF_2 substrate, which itself served as a source of fluorine (Fig. 1a). The fluorine released by the BaF_2 substrate was spatially confined to the narrow gap (typically 10–20 μm) between the Cu foil and the BaF_2 substrate (Supplementary Fig. 2). Fluorine was released in a very small, but sufficient, amount: in less than 1 min, the CVD growth of graphene on the front surface of the copper foil and that on the back surface—which is exposed to fluorine—were noticeably different. The graphene samples were grown in an atmospheric-pressure CVD system using CH_4 as the carbon source. On the back surface, circular graphene domains with lateral sizes of ~1 mm were observed. In contrast, on the front surface, star-like graphene domains formed that were only ~20 μm in size (Supplementary Fig. 3). Other metal fluoride substrates (CaF_2 and MgF_2) also led to the growth of circular graphene domains with a size of ~1 mm in a short time, verifying the sufficient supply of fluorine (Supplementary Fig. 4). As discussed in previous studies, the circular graphene domains are a result of the very high carbon flux and the attachment-limited growth behaviour[48]. To quantitatively analyse the growth rates on both surfaces, we first followed the established method to take images of graphene domains at different growth times Δt (Supplementary Note)[1,45]. $\Delta t = 0$ is defined as the moment when the graphene domains are clearly visualized by scanning electron microscopy (SEM) (~500 nm, shown in Supplementary Fig. 5). After an additional time Δt, we immediately stopped the furnace heating and CH_4 feeding, and flushed the samples with a large flux of Ar. The evolution of the graphene domains showed that 2 s was enough for a domain to grow to ~400 μm (Fig. 1b) and that ~1 mm domains were formed after 5 s (Fig. 1c). The statistical growth rate reached ~200 μm s^{-1} (Fig. 1d), which is more than three orders of magnitude faster than typical graphene growth[25–29] and three times faster than the previous record realized with a continuous oxygen supply[1].

To measure the growth rate of individual graphene domains, a carbon isotope labelling method can be used. A method widely used for this type of investigation comprises switching $^{12}CH_4$ and $^{13}CH_4$ with mass flow controllers during graphene growth[49]; the time-evolution of domain growth can then be visualized by Raman mapping due to the different peak positions of ^{12}C and ^{13}C. Because the growth rate is so high, isotope labelling must be performed in a few seconds, rendering this method impractical here ($^{13}CH_4$ and $^{12}CH_4$ would mix homogeneously before reaching the reaction site). Therefore, to separate the $^{12}CH_4$ and $^{13}CH_4$, a customized programmable transient pulse instrument was developed to inject sharp $^{13}CH_4$ pulses (10 ms) through a small pipe at a short time interval of 1–2 s (Fig. 1e; see Methods for details). After graphene growth, the transferred graphene samples on SiO_2/Si substrates are then characterized by Raman mapping[49] (Supplementary Fig. 6). With this improved isotope labelling method, the growth rate of graphene as a function of CH_4 flux could be measured (Supplementary Fig. 7). When the CH_4 flux was 2 s.c.c.m. (standard cubic centimetres per minute) and the pulse interval time was 2 s, the distance between adjacent ^{13}C rings in the Raman map was ~30 μm, revealing a lateral growth rate of ~30 μm s^{-1} (Fig. 1f). Under the optimum condition of graphene growth, by shortening the pulse interval time to 1 s, we measured

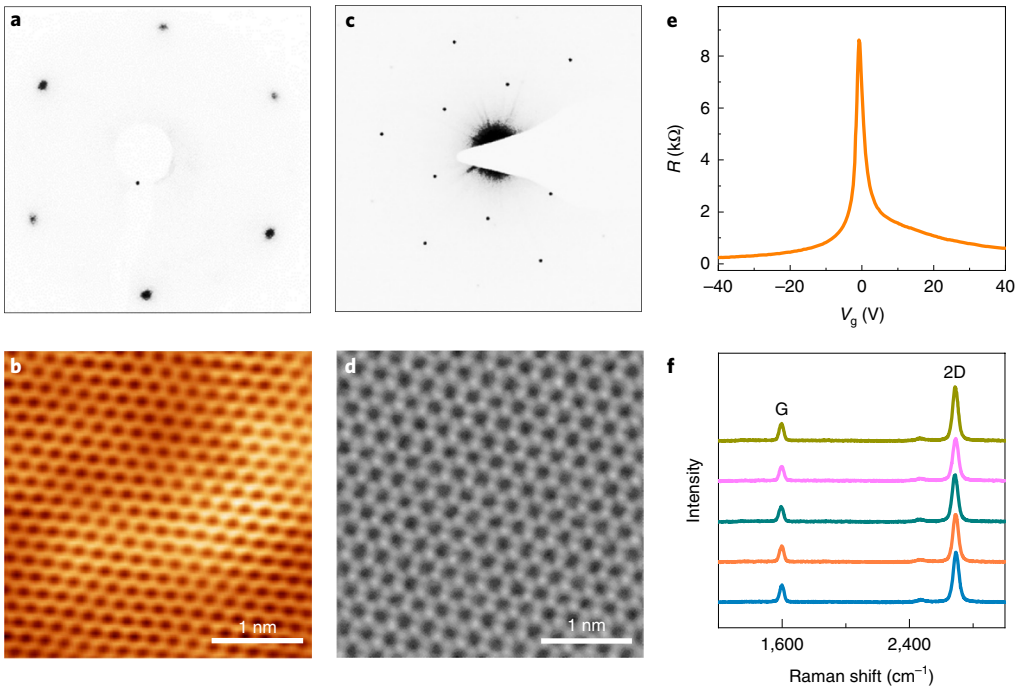

Fig. 2 | Crystallinity and quality characterizations of graphene domains. a,**b**, Representative LEED pattern (**a**) and STM image (**b**) of individual graphene domains, revealing the single-crystal characteristics of as-grown graphene domains. **c**,**d**, SAED pattern (**c**) and AC-STEM (**d**) image of a graphene domain, confirming the lattice structure of graphene. **e**, Resistance of graphene versus the back-gate voltage at 4 K, corresponding to an electron mobility of ~10,000 $cm^2 V^{-1} s^{-1}$. **f**, Representative Raman spectra of graphene without the D band, indicating the high quality of the material. Curves of different colours correspond to Raman spectra obtained at different positions of the sample.

a growth rate of ~190 $\mu m\, s^{-1}$ with a large CH_4 flux of 15 s.c.c.m. (Fig. 1g). It is important to note that further increasing the CH_4 flux led to contamination of the CVD system with amorphous carbon.

Crystallinity and quality characterizations of graphene domains. The graphene domains produced in the presence of fluorine released by the nearby BaF_2 substrate showed high crystallinity and quality, despite the significantly improved growth rate. We first characterized the lattice structure of graphene in reciprocal space by low-energy electron diffraction (LEED). The diffraction patterns in different areas of an individual graphene domain showed nearly identical crystallographic orientations (Fig. 2a and Supplementary Fig. 8), revealing the single-crystal nature of the circular domains. Scanning tunnelling microscopy (STM) characterization showed a honeycomb lattice without any detectable defects (Fig. 2b and Supplementary Fig. 9), indicating no contamination in the graphene lattice. Selected-area electron diffraction (SAED) and spherical aberration-corrected scanning transmission electron microscopy (AC-STEM) were also performed to confirm the good crystallinity of the graphene with diffraction patterns and the atomic-resolved lattice structure (Fig. 2c,d). The measured Hall mobility of the graphene transferred onto h-BN is ~10,000 $cm^2 V^{-1} s^{-1}$ at 4 K, which is comparable to that of exfoliated graphene subjected to the same transfer process[1] (Fig. 2e). In addition, the fact that the Raman spectra do not show a D band—which would correspond to the disordered structure in a graphene lattice—further confirms the high quality of the material (Fig. 2f). The 2D/G intensity, which is very sensitive to the thickness of graphene, shows a ratio of ~2 in the Raman spectra, and the uniform brightness and contrast in the SEM images demonstrate the monolayer nature of the graphene domains and films (Supplementary Fig. 10). The XPS measurement shows no detectable fluorine signal (Supplementary Fig. 11), indicating that the as-grown graphene samples are not F-doped.

Mechanism for the local fluorine-modulated superfast graphene growth. To understand the role of spatially confined fluorine in the modulation of graphene growth, we first considered two possible mechanisms: (1) fluorine can promote CH_4 decomposition on the Cu surface (in a similar manner to the role of oxygen in graphene growth, as reported previously[1,2]) or (2) CH_4 decomposition can occur directly on the metal fluoride surface. We carried out extensive density functional theory (DFT) calculations, which showed that fluorine on the Cu surface does not significantly accelerate the decomposition of CH_4 (Supplementary Fig. 12) and that the decomposition of CH_4 on the BaF_2 surface is even more difficult than that on the Cu surface (Supplementary Fig. 13).

We next considered the gas-phase reactions, and noticed that the fluorine released from the metal fluoride surface can substitute the hydrogen in CH_4 to form CH_3F easily[50,51] (route I, Fig. 3a), potentially leading to a high concentration of CH_3F in the narrow gap between the Cu and the metal fluoride surface (Fig. 3a,b). Further calculations showed that the decomposition of CH_3F on the Cu surface (route II, Fig. 3a) is much easier than that of CH_4 on Cu (Fig. 3c). In addition to its role in decreasing the energy barrier of CH_4 decomposition on the Cu surface, in a manner similar to that for oxygen, the formation of CH_3F was also found to switch the originally endothermic reaction to an exothermic one. We note that reaction II with a barrier of 1.24 eV can occur very frequently at ~1,000 °C. Therefore, with such a low reaction energy (−0.62 eV), we conclude that the concentration of CH_3 radicals can be greatly promoted by the direct decomposition of CH_3F on the Cu surface.

It is also worth noting that, at ~1,000 °C, entropy must contribute a significant part to the initial configuration, final product or transition state of a reaction. Careful calculations considering the vibrational entropy (Supplementary Figs. 14 and 15 and Supplementary Tables 1 and 2) confirmed that the entropy indeed largely contributed to the free energy of each state of the reaction at ~1,000 °C.

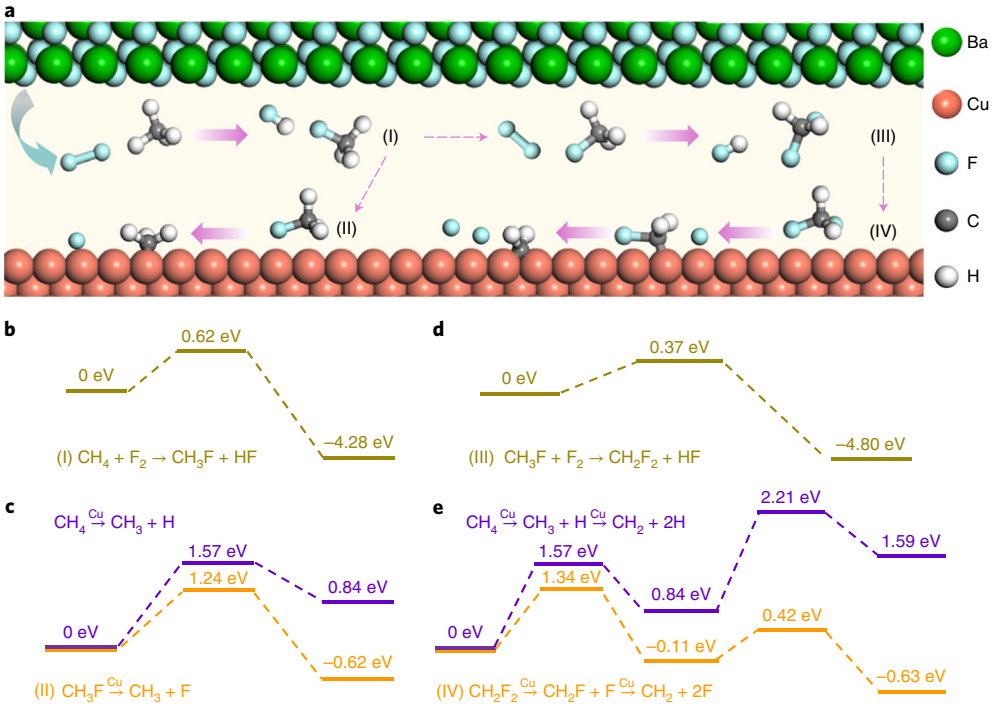

Fig. 3 | Proposed mechanism for local fluorine-modulated graphene growth. a, Schematics of the two possible decomposition routes of carbon species in the gas phase (I and III) and on the Cu surface (II and IV). **b**, Energy profile for route I: $CH_4 + F_2 \rightarrow CH_3F + HF$. **c**, Energy profile for two reactions on the Cu surface: decomposition of CH_3F to CH_3 (orange) and CH_4 to CH_3 (violet). **d**, Energy profile for route III: $CH_3F + F_2 \rightarrow CH_2F_2 + HF$. **e**, Energy profile for two reactions on the Cu surface: decomposition of CH_2F_2 to CH_2 (orange) and CH_4 to CH_2 (violet). Compared to the CH_4 decomposition, the fluorine-modulated reactions have lower barriers and reaction kinetics that switch from endothermic to highly exothermic; both factors lead to a greatly elevated concentration of reactive carbon species and, consequently, superfast graphene growth.

Nevertheless, the entropy contributions to all three states of the reaction are of very similar magnitude to each other and thus do not dramatically affect the reaction barrier and the reaction energy, so they do not affect the main conclusion that a high concentration of CH_3 radicals can be obtained with released fluorine.

Similarly, DFT calculations showed that the formation of CH_2F_2 (route III, Fig. 3a) is also highly favourable (Fig. 3d). The further decomposition of CH_2F_2 (route IV, Fig. 3a) is also an exothermic reaction for the decomposition of CH_2F_2 to CH_2 on the Cu surface (Fig. 3e). Therefore, as fluorine substitution in the gas phase and further decomposition reactions on the Cu surface can both occur easily, a high concentration of CH_x ($x = 1, 2, 3$) radicals on the Cu surface or in the gas phase is expected. The graphene growth would then be significantly promoted by a sufficient supply of CH_x radicals.

Modulated growth of 2D h-BN and WS_2 by a local fluorine supply. We next investigated whether local fluorine could also serve to modulate the growth of 2D materials other than graphene—here, h-BN and WS_2. In a CVD set-up similar to that used for graphene growth, for h-BN growth a Cu foil was placed above a BaF_2 substrate (Fig. 4a). At high temperatures, the released fluorine can directly participate in the decomposition of ammonia borane (H_3BNH_3) and the growth process of h-BN on the Cu surface facing the metal fluoride.

In this case too, the growth kinetics of h-BN were significantly altered in proximity to the BaF_2 substrate, and the domain size is approximately ten times larger than that grown without a fluorine supply (Fig. 4b,c and Supplementary Fig. 16), indicating a faster growth rate (3.3 μm min^{-1} compared with 0.3 μm min^{-1} for growth without a fluorine supply).

The growth conditions for WS_2 are different from those of graphene or h-BN. WO_3 and S powder (as precursors) and WS_2 were deposited on the SiO_2/Si substrate downstream. Among the growth steps for WS_2, evaporation of WO_3 is key in determining intermediate formation and the growth rate, so fluorine was introduced by placing the WO_3 powder on the BaF_2 substrate (Fig. 4d). Surprisingly, with such a small modification the domain size of the WS_2 increased from ~1 μm to ~100 μm, and the growth rate increased from 0.2 μm min^{-1} to 20 μm min^{-1} (Fig. 4e,f and Supplementary Fig. 17). We also observed an enhanced growth rate for $MoSe_2$ with fluorine (Supplementary Fig. 18). This phenomenon is similar to the NaCl-assisted growth of 2D metal chalcogenides, where NaCl decreases the melting point of the reactants and facilitates the formation of intermediate products, increasing the overall reaction rate[52]. Although the detailed mechanism of the enhanced growth of h-BN and WS_2 needs further study, it is clear that the introduction of fluorine significantly modifies key reactions involved in their growth. We speculate that fluorine can facilitate H_3BNH_3 decomposition in h-BN growth and lead to the fast release of W in WS_2 growth.

Discussion

We have described kinetic modulation of the CVD growth of three representative 2D materials—conductive graphene, insulating h-BN and semiconducting WS_2—by spatially confined fluorine. We found that local fluorine effectively switches the kinetic reaction of methane decomposition in graphene CVD growth from endothermic to exothermic, leading to a high growth rate of ~200 μm s^{-1}. Similarly, in the presence of fluorine, 2D h-BN and WS_2 were found to grow more quickly. Although further investigations into the mechanisms of h-BN and WS_2 growth are required, it is clear that

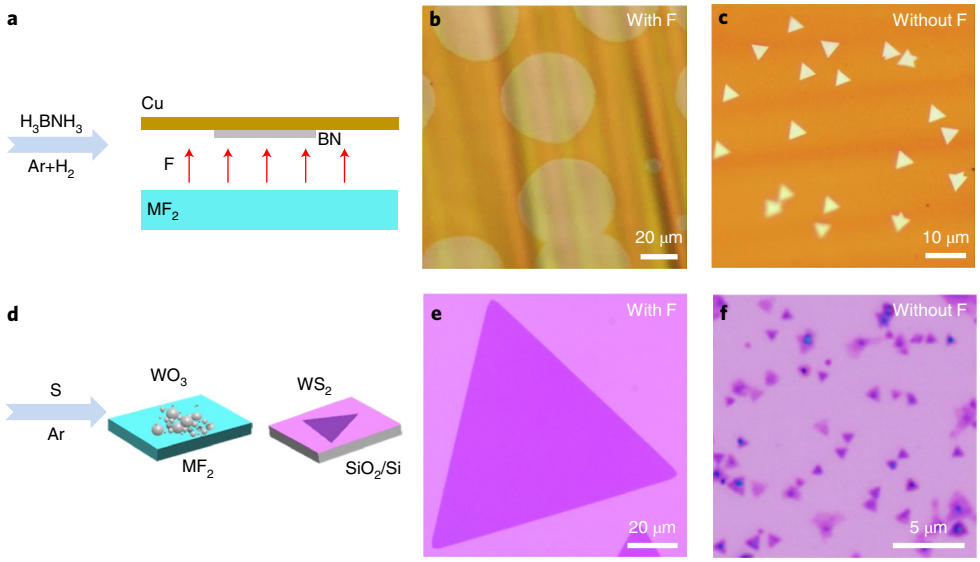

Fig. 4 | Modulated growth of 2D h-BN and WS_2 by a local fluorine supply. a, Schematics of the experimental design for h-BN growth. Different feeding gases are used, but the growth process for this material is similar to that observed for graphene. **b**,**c**, Optical images of the h-BN domains on Cu surfaces (after heating in air at 150 °C for 2 min) with (**b**) and without (**c**) a local fluorine supply for the same growth time. The domain size of the resulting h-BN domain increased from ~5 μm to ~50 μm with the fluorine supply. **d**, Schematics of the experimental design for WS_2 growth; the WO_3 precursor powder is directly placed on a BaF_2 substrate. **e**,**f**, Optical images of the WS_2 domains on SiO_2/Si substrates with (**e**) and without (**f**) a fluorine supply for the same growth time. The size of the WS_2 domain increased from ~1 μm to ~100 μm in the presence of fluorine during the reaction.

the small amount of local fluorine generated from a metal fluoride is sufficient to modulate the growth in two dimensions while being low enough not to damage the reactors.

We also hope that the idea of introducing local active species into certain reaction processes can be used to further tune 2D material synthesis and enable fast growth, low-temperature growth, in situ element doping and perhaps also the growth of super-large single crystals if one can control the growth from only one nucleus or grow them epitaxially on certain substrates. In addition to metal fluorides, materials such as metal sulfides, selenides, chlorides and bromides may similarly be used as sources of active species. These substrates have different abilities to capture electrons and variable reactivity, and they release elements over a broad range of temperatures (~50–1,400 °C). Therefore, this local active element supply technique may provide a versatile platform to modulate the growth of 2D materials and engineer their properties (for example, electronic, optical, thermal, magnetic and catalytic).

Methods

Growth of graphene by a local fluorine supply. Graphene samples were grown by the CVD method. A commercially available Cu foil (25 or 127 μm thick, 99.8%, Alfa Aesar) was placed on a metal fluoride substrate and then loaded into a CVD furnace (Hefei Kejing Company OTF1250). The system was heated to 1,000 °C in 1 h with Ar (500 s.c.c.m.). H_2 (10 s.c.c.m.) and CH_4 (2–15 s.c.c.m.) were then introduced to achieve graphene growth of different durations. Finally, the system was cooled rapidly with a large flux of Ar (1,000 s.c.c.m.).

Growth of h-BN by a local fluorine supply. h-BN samples were grown by the CVD method. The system was heated to 1,000 °C in 1 h with Ar (500 s.c.c.m.). Afterwards, the system was switched to a low pressure of 180 Pa with Ar (20 s.c.c.m.) and H_2 (3 s.c.c.m.), while the vapourized H_3BNH_3, nested in an Al_2O_3 crucible and heated to 120 °C by heating belts, was introduced as a precursor for h-BN growth. After 15 min of growth, both the furnace and the heating belts were rapidly cooled to room temperature.

Growth of WS_2 by a local fluorine supply. WS_2 on the SiO_2/Si substrate was grown by the CVD method using WO_3 and S powder as precursors. 10 mg of WO_3 powder was placed on the BaF_2 substrate in the centre of a tube furnace, and 20 mg of S powder was placed on the upstream side 15 cm away from the WO_3 powder. The growth was performed under ambient pressure in Ar gas. The procedure was as follows: maintain at 105 °C with 500 s.c.c.m. Ar flow for 30 min, ramp to 850 °C with 15 s.c.c.m. Ar flow for 45 min, maintain at 850 °C with 250 s.c.c.m. Ar flow for 5 min, and then naturally cool to room temperature with 500 s.c.c.m. Ar flow.

Programmable local transient pulse set-up. The Cu foil was exposed to $^{12}CH_4$ at constant flux, and a small flux of $^{13}CH_4$ was introduced by a small nozzle (diameter of 1 mm) focused on the gap between the Cu foil and the fluoride substrate. The $^{13}CH_4$ supply was controlled by a programmable transient pulse instrument, which can control the pulse width to be as sharp as 10 ms and the pulse interval to be as low as 1 s. This sensitive control separated the $^{13}CH_4$ flux into sequences. These sequences of $^{13}CH_4$ flux were further separated in space by a large Ar flow in the pipe. We used the shortest pipelines and nozzle available for the $^{13}CH_4$ flow to minimize the gas diffusion time.

Graphene characterization. *Optical measurements.* Raman mappings of graphene on SiO_2/Si substrates were as carried out in an Alpha300R system (WITec, Germany) with a laser excitation wavelength of 532 nm and a power of 1 mW. The integral time of every point was 0.05 s during mapping. Optical images were taken with an Olympus microscope (Olympus BX51). UV–vis spectra were obtained with a Varian Cary 5000 UV–vis–NIR spectrophotometer.

XPS, LEED, STM and TEM measurements. XPS measurements were performed using an ESCALAB 250 X system (Thermo Fisher Scientific) and excited by monochromatic Al Kα radiation (1,486.6 eV). LEED measurements were performed using an Omicron LEED system under ultrahigh vacuum (UHV) with a base pressure below 3×10^{-7} Pa and an electron energy of 62 eV. STM experiments were performed with a combined nc-AFM/STM system (Createc) at 77 K with a base pressure of 6×10^{-9} Pa. AC-STEM experiments were performed in a JEOL JEM ARM 300F under 80 kV with a low electron dose to minimize beam damage. Diffraction patterns were obtained with an FEI TECNAI F20 system operated at 200 kV.

DFT calculations. *Calculation models.* Metal surfaces were simulated by a four-atom-layer slab of the Cu(100) surface with 4×4 Cu atoms on the *x*–*y* plane using the periodic boundary condition. The supercell was 10.2×10.2 Å^2 in size. The metal fluoride surface was modelled by a three-atom-layer slab model of the BaF_2(111) surface with 3×3 Ba atoms (13.1×13.1 Å^2 size) on the *x*–*y* plane. To avoid interaction between neighbouring slabs, a vacuum layer greater than 10 Å was inserted to ensure periodicity along the *z* direction. During structure optimization, all the atoms of the bottom layer were fixed while the others were fully relaxed.

Calculation details. All calculations were performed using the Vienna ab initio Simulation Package (VASP)[53–55] with the project augmented wave (PAW) method[56]. The generalized gradient approximation (GGA) with the Perdew–Burke–Ernzerhof

exchange-correlation functional was adopted[57]. A plane-wave energy cutoff of 400 eV was used and all the structures were fully relaxed with energy and force convergence criteria of 10^{-4} eV and 10^{-2} eV Å^{-1}, respectively. The transition barriers and minimum energy paths were calculated with the climbing image nudged elastic band method[53,56,58].

Data availability

The data supporting the findings of this study are available within the paper and its Supplementary Information, and also from the authors upon request.

Received: 4 June 2018; Accepted: 30 May 2019;
Published online: 15 July 2019

References

1. Xu, X. Z. et al. Ultrafast growth of single-crystal graphene assisted by a continuous oxygen supply. *Nat. Nanotechnol.* **11**, 930–935 (2016).
2. Hao, Y. F. et al. The role of surface oxygen in the growth of large single-crystal graphene on copper. *Science* **342**, 720–723 (2013).
3. Hao, Y. F. et al. Oxygen-activated growth and bandgap tunability of large single-crystal bilayer graphene. *Nat. Nanotechnol.* **11**, 426–431 (2016).
4. Kiplinger, J. L., Richmond, T. G. & Osterberg, C. E. Activation of carbon fluorine bonds by metal-complexes. *Chem. Rev.* **94**, 373–431 (1994).
5. Reichenbacher, K., Suss, H. I. & Hulliger, J. Fluorine in crystal engineering—'the little atom that could'. *Chem. Soc. Rev.* **34**, 22–30 (2005).
6. Muller, K., Faeh, C. & Diederich, F. Fluorine in pharmaceuticals: looking beyond intuition. *Science* **317**, 1881–1886 (2007).
7. Purser, S., Moore, P. R., Swallow, S. & Gouverneur, V. Fluorine in medicinal chemistry. *Chem. Soc. Rev.* **37**, 320–330 (2008).
8. Price, S. C. et al. Fluorine substituted conjugated polymer of medium band gap yields 7% efficiency in polymer–fullerene solar cells. *J. Am. Chem. Soc.* **133**, 4625–4631 (2011).
9. Furuya, T., Kamlet, A. S. & Ritter, T. Catalysis for fluorination and trifluoromethylation. *Nature* **473**, 470–477 (2011).
10. Nair, R. R. et al. Fluorographene: a two-dimensional counterpart of teflon. *Small* **6**, 2877–2884 (2010).
11. Zboril, R. et al. Graphene fluoride: a stable stoichiometric graphene derivative and its chemical conversion to graphene. *Small* **6**, 2885–2891 (2010).
12. Romero-Aburto, R. et al. Fluorinated graphene oxide; a new multimodal material for biological applications. *Adv. Mater.* **25**, 5632–5637 (2013).
13. Castro Neto, A. H. et al. The electronic properties of graphene. *Rev. Mod. Phys.* **81**, 109–162 (2009).
14. Chhowalla, M. et al. The chemistry of two-dimensional layered transition metal dichalcogenide nanosheets. *Nat. Chem.* **5**, 263–275 (2013).
15. Giles, A. J. et al. Ultralow-loss polaritons in isotopically pure boron nitride. *Nat. Mater.* **17**, 134–139 (2018).
16. Kubota, Y., Watanabe, K., Tsuda, O. & Taniguchi, T. Deep ultraviolet light-emitting hexagonal boron nitride synthesized at atmospheric pressure. *Science* **317**, 932–934 (2007).
17. Novoselov, K. S. et al. A roadmap for graphene. *Nature* **490**, 192–200 (2012).
18. Wang, Q. H. et al. Electronics and optoelectronics of two-dimensional transition metal dichalcogenides. *Nat. Nanotechnol.* **7**, 699–712 (2012).
19. Young, R. J. Two-dimensional nanocrystals: structure, properties and applications. *Arab. J. Sci. Eng.* **38**, 1289–1304 (2013).
20. Fiori, G. et al. Electronics based on two-dimensional materials. *Nat. Nanotechnol.* **9**, 768–779 (2014).
21. Cho, S. et al. Phase patterning for ohmic homojunction contact in $MoTe_2$. *Science* **349**, 625–628 (2015).
22. Keum, D. H. et al. Bandgap opening in few-layered monoclinic $MoTe_2$. *Nat. Phys.* **11**, 482–486 (2015).
23. Yang, H., Kim, S. W., Chhowalla, M. & Lee, Y. H. Structural and quantum-state phase transitions in van der Waals layered materials. *Nat. Phys.* **13**, 1232–1232 (2017).
24. Dai, B. Y. et al. Rational design of a binary metal alloy for chemical vapour deposition growth of uniform single-layer graphene. *Nat. Commun.* **2**, 522 (2011).
25. Gao, L. et al. Repeated growth and bubbling transfer of graphene with millimetre-size single-crystal grains using platinum. *Nat. Commun.* **3**, 699 (2012).
26. Geng, D. C. et al. Uniform hexagonal graphene flakes and films grown on liquid copper surface. *Proc. Natl Acad. Sci. USA* **109**, 7992–7996 (2012).
27. Yan, Z. et al. Toward the synthesis of wafer-scale single-crystal graphene on copper foils. *ACS Nano* **6**, 9110–9117 (2012).
28. Zhou, H. L. et al. Chemical vapour deposition growth of large single crystals of monolayer and bilayer graphene. *Nat. Commun.* **4**, 2096 (2013).
29. Lee, J. H. et al. Wafer-scale growth of single-crystal monolayer graphene on reusable hydrogen-terminated germanium. *Science* **344**, 286–289 (2014).
30. Gao, L. B. et al. Face-to-face transfer of wafer-scale graphene films. *Nature* **505**, 190–194 (2014).
31. Babenko, V. et al. Rapid epitaxy-free graphene synthesis on silicidated polycrystalline platinum. *Nat. Commun.* **6**, 7536 (2015).
32. Nguyen, V. L. et al. Seamless stitching of graphene domains on polished copper (111) foil. *Adv. Mater.* **27**, 1376–1382 (2015).
33. Wu, T. R. et al. Fast growth of inch-sized single-crystalline graphene from a controlled single nucleus on Cu–Ni alloys. *Nat. Mater.* **15**, 43–47 (2016).
34. Wang, Z. J. et al. Stacking sequence and interlayer coupling in few-layer graphene revealed by in situ imaging. *Nat. Commun.* **7**, 13256 (2016).
35. Wang, H. et al. Surface monocrystallization of copper foil for fast growth of large single-crystal graphene under free molecular flow. *Adv. Mater.* **28**, 8968–8974 (2016).
36. Zhang, Z. H. et al. The way towards ultrafast growth of single-crystal graphene on copper. *Adv. Sci.* **4**, 1700087 (2017).
37. Xu, X. Z. et al. Ultrafast epitaxial growth of metre-sized single-crystal graphene on industrial Cu foil. *Sci. Bull.* **62**, 1074–1080 (2017).
38. Vlassiouk, I. V. et al. Evolutionary selection growth of two-dimensional materials on polycrystalline substrates. *Nat. Mater.* **17**, 318–322 (2018).
39. Liu, Z. et al. In-plane heterostructures of graphene and hexagonal boron nitride with controlled domain sizes. *Nat. Nanotechnol.* **8**, 119–124 (2013).
40. Liu, L. et al. Heteroepitaxial growth of two-dimensional hexagonal boron nitride templated by graphene edges. *Science* **343**, 163–167 (2014).
41. Duan, X. D. et al. Lateral epitaxial growth of two-dimensional layered semiconductor heterojunctions. *Nat. Nanotechnol.* **9**, 1024–1030 (2014).
42. Yin, J. et al. Large single-crystal hexagonal boron nitride monolayer domains with controlled morphology and straight merging boundaries. *Small* **11**, 4497–4502 (2015).
43. Kang, K. et al. High-mobility three-atom-thick semiconducting films with wafer-scale homogeneity. *Nature* **520**, 656–660 (2015).
44. Lu, G. Y. et al. Synthesis of large single-crystal hexagonal boron nitride grains on Cu–Ni alloy. *Nat. Commun.* **6**, 6160 (2015).
45. Gao, Y. et al. Ultrafast growth of high-quality monolayer WSe_2 on Au. *Adv. Mater.* **29**, 1700990 (2017).
46. Zhang, Z. W. et al. Robust epitaxial growth of two-dimensional heterostructures, multiheterostructures and superlattices. *Science* **357**, 788–792 (2017).
47. Wang, H. et al. High-quality monolayer superconductor $NbSe_2$ grown by chemical vapour deposition. *Nat. Commun.* **8**, 394 (2017).
48. Dong, J., Zhang, L. & Ding, F. Kinetics of graphene and 2D materials growth. *Adv. Mater.* **31**, 1801583 (2019).
49. Li, X. S., Cai, W. W., Colombo, L. & Ruoff, R. S. Evolution of graphene growth on Ni and Cu by carbon isotope labeling. *Nano Lett.* **9**, 4268–4272 (2009).
50. Moss, J. H., Ottie, R. & Wilford, J. B. The fluorination of methane and related compounds by copper(II) fluoride and other metal fluorides. *J. Fluor. Chem.* **6**, 393–416 (1975).
51. Kaneko, C. et al. Reaction of methane with molecular fluorine: an ab initio MO study. *Chem. Pharm. Bull.* **42**, 745–747 (1994).
52. Zhou, J. D. et al. A library of atomically thin metal chalcogenides. *Nature* **556**, 355–359 (2018).
53. Kresse, G. & Furthmuller, J. Efficiency of ab-initio total energy calculations for metals and semiconductors using a plane-wave basis set. *Comp. Mater. Sci.* **6**, 15–50 (1996).
54. Kresse, G. & Hafner, J. Ab-initio molecular-dynamics for open-shell transition-metals. *Phys. Rev. B.* **48**, 13115–13118 (1993).
55. Wu, P. et al. Carbon dimers as the dominant feeding species in epitaxial growth and morphological phase transition of graphene on different Cu substrates. *Phys. Rev. Lett.* **114**, 216102 (2015).
56. Henkelman, G., Uberuaga, B. P. & Jonsson, H. A climbing image nudged elastic band method for finding saddle points and minimum energy paths. *J. Chem. Phys.* **113**, 9901–9904 (2000).
57. Perdew, J. P., Burke, K. & Ernzerhof, M. Generalized gradient approximation made simple. *Phys. Rev. Lett.* **77**, 3865–3868 (1996).
58. Kresse, G. & Joubert, D. From ultrasoft pseudopotentials to the projector augmented-wave method. *Phys. Rev. B.* **59**, 1758–1775 (1999).

Acknowledgements

This work was supported by the National Key R&D Program of China (2016YFA0300903, 2016YFA0300804 and 2015CB358600), the NSFC (51522201, 11474006 and 51722204), the National Equipment Program of China (ZDYZ2015-1), Beijing Municipal Science & Technology Commission (Z181100004218006), Beijing Graphene Innovation Program (Z181100004818003 and Z161100002116028), the Bureau of Industry and Information Technology of Shenzhen (Graphene Platform contract no. 201901161512), the Science–Technology and Innovation Commission of Shenzhen Municipality (ZDSYS20170303165926217 and JCYJ20170412152620376), the Economic–Trade and Information Commission of Shenzhen Municipality, Guangdong Innovative and Entrepreneurial Research Team Program (2016ZT06D348), the National Postdoctoral Program for Innovative Talents (BX201700014 and

BX20190016), the Fundamental Research Funds for the Central Universities (ZYGX2016Z004), the Institute for Basic Science (IBS-R019-D1) of South Korea and the Outstanding Research Fund (1.180066.01) of UNIST (Ulsan National Institute of Science & Technology).

Author contributions

K.L., E.W., D.Y. and C.L. conceived the experiment. K.L., F.D. and J.X. supervised the project. C.L., X.X. and M.W. conducted the growth experiment. C.L. performed Raman and XPS experiments. X.X. and Y.J. performed LEED and STM experiments. R.Q. and P.G. conducted the TEM experiments. J.N. and X.W. performed the electrical measurements. F.D. and L.Q. performed theoretical calculations. All of the authors discussed the results and wrote the paper.

Competing interests

The authors declare no competing interests.

Additional information

Supplementary information is available for this paper at https://doi.org/10.1038/s41557-019-0290-1.

Reprints and permissions information is available at www.nature.com/reprints.

Correspondence and requests for materials should be addressed to J.X., F.D. or K.L.

Publisher's note: Springer Nature remains neutral with regard to jurisdictional claims in published maps and institutional affiliations.